Hydrological deformation induced by the West African Monsoon: Comparison of GPS, GRACE and loading models

Samuel Nahmani,[1] Olivier Bock,[1] Marie-Noëlle Bouin,[2] Alvaro Santamaría-Gómez,[3] Jean-Paul Boy,[4] Xavier Collilieux,[1] Laurent Métivier,[1,5] Isabelle Panet,[1,5] Pierre Genthon,[6] Caroline de Linage,[7] and Guy Wöppelmann[8]

Received 16 December 2011; revised 25 March 2012; accepted 27 March 2012; published 12 May 2012.

[1] Three-dimensional ground deformation measured with permanent GPS stations in West Africa was used for investigating the hydrological loading deformation associated with Monsoon precipitation. The GPS data were processed within a global network for the 2003–2008 period. Weekly station positions were retrieved with a repeatability (including unmodeled loading effects) of 1–2 mm in the horizontal components and between 2.5 and 6 mm in the vertical component. The annual signal in the vertical component for sites located between 9.6°N and 16.7°N is in the range 10–15 mm. It is consistent at the 3 mm-level with the annual regional-scale loading deformations estimated from GRACE satellite products and modeled with a combination of hydrological, atmospheric, and nontidal oceanic models. An additional 6 month transient signal was detected in the vertical component of GPS estimates at most of the West African sites. It takes the form of an oscillation occurring between September and March, and reaching a maximum amplitude of 12–16 mm at Ouagadougou (12.5°N). The analysis of in situ hydro-geological data revealed a strong coincidence between this transient signal and peak river discharge at three sites located along the Niger River (Timbuktu, Gao, and Niamey). At Ouagadougou, a similar coincidence was found with the seasonal variations of the water table depth. We propose a mechanism to account for this signal that involves a sequence of swelling/shrinking of clays combined with local loading effects associated with flooding of the Niger River.

Citation: Nahmani, S., et al. (2012), Hydrological deformation induced by the West African Monsoon: Comparison of GPS, GRACE and loading models, *J. Geophys. Res.*, *117*, B05409, doi:10.1029/2011JB009102.

1. Introduction

[2] Terrestrial water storage is a key component of global hydrological cycles [*Syed et al.*, 2008]. The primary objective of the Gravity Recovery And Climate Experiment (GRACE) satellite mission launched in 2002 was to monitor the hydrological mass redistributions through their integrated gravitational effect, with a spatial resolution close to 400 km and with monthly down to 1 day time periods [*Tapley et al.*, 2004; *Kusche and Schrama*, 2005]. The unprecedented accuracy of these gravity field time variations enables us to monitor geophysical processes, such as water storage change, which is the dominant source of mass variation at the seasonal timescale [*Wahr et al.*, 2004; *Schmidt et al.*, 2006]. GRACE products are well-adapted to the monitoring of basin up to global scales; they can also be used to validate and to improve hydrological land surface models.

[3] A number of past studies adopted a global perspective and presented information susceptible to aid flood forecasting over several large river basins [e.g., *Reager and Famiglietti*, 2009]. Others focused on one large basin, like the Amazon Basin [*Crowley et al.*, 2008; *Han et al.*, 2010] or the Congo Basin [*Crowley et al.*, 2006] to extract annual, semiannual and long-term trends of the continental water mass variation. Most of these studies compared GRACE signals with hydrological land surface model predictions, as GRACE data sets also constitute a unique opportunity to validate and to improve models. The main results of these global inter-comparison studies over major river basins [e.g., *Ramillien et al.*, 2005; *Schmidt et al.*, 2008; *Syed et al.*, 2008; *Han et al.*, 2010] showed a generally high level of agreement regarding the magnitude of semiannual and annual terms, and of inter-annual variations, with some underestimation of the seasonal amplitude of water storage in the model predictions.

[1]LAREG/GRGS, IGN, Marne La Vallée, France.
[2]Centre de Météorologie Marine, CNRM, Brest, France.
[3]Instituto Geográfico Nacional, Yebes, Spain.
[4]EOST-IPGS, UMR 7516, CNRS-UdS, Université de Strasbourg, Strasbourg, France.
[5]Institut de Physique du Globe de Paris, Université Paris-Diderot, UMR 7154, Paris, France.
[6]IRD/Hydrosciences Montpellier, Université de Montpellier, Montpellier, France.
[7]Earth System Science, University of California, Irvine, USA.
[8]LIENSS, Université de La Rochelle, CNRS, La Rochelle, France.

Corresponding author: S. Nahmani, LAREG/GRGS, IGN, 6-8 ave. Blaise Pascal, F-77455 Marne La Vallée Cedex 2, France. (samuel.nahmani@ign.fr)

0148-0227/12/2011JB009102

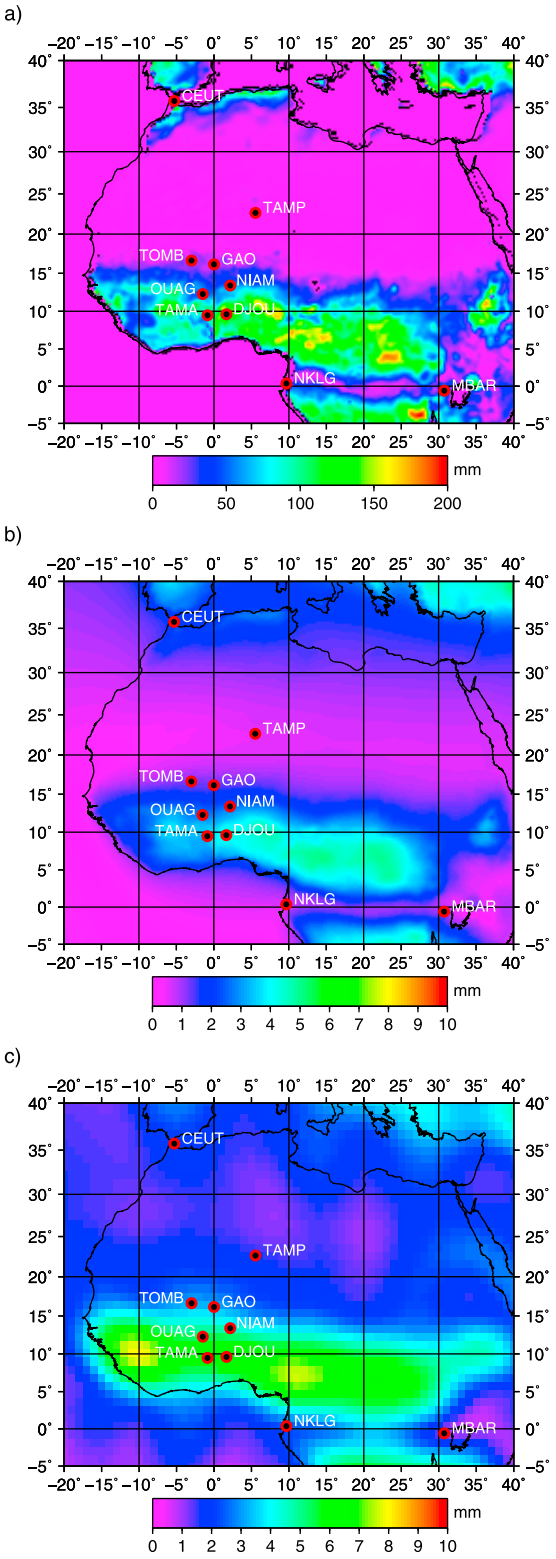

Figure 1. Amplitude of the annual harmonic of (a) soil moisture modeled by GLDAS/NOAH, (b) elastic vertical deformation estimated from GLDAS/NOAH simulations in the CF frame, (c) elastic vertical deformation estimated from GRACE data in the CF frame. GPS permanent stations are shown as red-black circles with their four letter acronyms. Units: soil moisture (mm), vertical deformation (mm).

Models also showed less variability at the monthly timescale, and exhibited a systematic advance of phase in the annual term as compared to GRACE products, in the range of 1 to 6 weeks [*Schmidt et al.*, 2008]. These discrepancies were attributed to model deficiencies in the surface water storage representation (runoff and horizontal transport terms). It should be noted, however, that the GRACE products used for these comparisons originated from several processing centers and included various correcting terms and filtering approaches. The reader may refer to *Güntner* [2008] for a review of studies comparing GRACE products with simulation outputs of global hydrological models.

[4] The aim of this study is to assess whether Global Positioning System (GPS) derived ground deformation could help to fill the gap between the information contained in GRACE products and model simulations in West Africa. Over the past 5–6 years, West Africa has been the focus of intensive scientific experimental campaigns within the framework of AMMA (African Monsoon Multidisciplinary Analysis) and GHYRAF (Gravity and Hydrology in Africa) projects. AMMA is a major international scientific program devoted to improving our understanding of the West African Monsoon system as well as its environmental and socio-economic impacts [*Redelsperger et al.*, 2006; *Lebel et al.*, 2009]. GHYRAF is a French project designed to study the continental water cycle in West Africa, using ground-based and spaceborne gravity data in addition to GPS and more conventional geophysical and hydrological observations and modeling [*Hinderer et al.*, 2009].

[5] Figure 1a shows the annual amplitude of the soil moisture simulated with the Global Land Data Assimilation System (GLDAS) hydrology model (Noah release) [*Rodell et al.*, 2004]. Figures 1b and 1c show the annual amplitudes of the vertical deformation from the GLDAS model outputs and from the GRACE products from Centre National des Etudes Spatiales/Groupe de Recherche en Géodésie Spatiale (CNES/GRGS), release-2 [*Bruinsma et al.*, 2010]. In good consistency with the results of *Schmidt et al.* [2008] and *Grippa et al.* [2011], the GRACE annual amplitude is larger than that of the model. Six GPS stations were set up in West Africa within the framework of AMMA [*Bock et al.*, 2008]. They are located in the main monsoon area. Thus, they are well-adapted for monitoring the strong latitudinal variability of the land water changes in connection with the monsoon dynamics. The difference between the GRACE and model deformation estimates is larger than the uncertainty of the GPS position estimates, which makes the analysis of the combination of these three techniques especially interesting.

[6] Since the beginning of the GRACE era, several studies examined existing permanent GPS networks to compare and somehow validate the hydrological signals of GRACE products and/or model simulations [e.g., *Davis et al.*, 2004; *Kusche and Schrama*, 2005; *King et al.*, 2006; *van Dam et al.*, 2007; *Tregoning et al.*, 2009; *Steckler et al.*, 2010; *Tesmer et al.*, 2011]. At a global scale, using GPS position time series provided by the IGS service, *Kusche and Schrama* [2005] found a good agreement between the annual variations of continental water mass seen by GPS or GRACE and those predicted by a global hydrological model. More recently, *Tregoning et al.* [2009] computed elastic deformations using continental water storage variations derived from GRACE products. Then, they compared them with 3-D deformations

estimated from a global reprocessed GPS network including 80 sites. They obtained a general good agreement between the two data sets, with the Root-Mean-Square (RMS) of GPS coordinate anomalies decreasing at ∼50% of their sites when the GRACE derived deformation estimates were subtracted from their GPS solution. The fit was especially good on European stations with 32 out of 36 stations showing a decrease of RMS anomalies. This was in contrast with previous results over the same area [*van Dam et al.*, 2007]. The reprocessing of GPS observations using the latest standards was presented as an explanation of this improvement. *Tesmer et al.* [2011] used more or less the same approach over a larger global network of 115 stations; they used longer data sets both for GRACE and GPS products (September 2002 to April 2009). They obtained improved results in comparison with previous global studies since 80% of their stations showed a decrease of RMS anomalies. Interestingly, they estimated the precision of the GRACE-derived deformations at ∼1.2 mm through a comparison between 3 different GRACE products.

[7] *Grippa et al.* [2011] focused more specifically on West Africa and compared land water storage estimates from six GRACE products and soil moisture estimates from nine hydrological land surface models over the 2003–2007 period. They provided a thorough analysis of the annual water cycle, of the inter-annual variations, and of the latitudinal distribution of water storage. The GRACE products all showed quite consistent changes over time, with water maxima observed in September and minima in April. However, discrepancies were evident in the amplitudes of the annual water storage variations. The models showed a consistent latitudinal distribution in soil moisture and time changes, but there were significant differences in the amplitude of seasonal variations in soil moisture. These model simulations were performed within the AMMA Land Surface Inter-comparison Project (ALMIP) [*Boone et al.*, 2009] using the same forcings (precipitation, radiation at the surface and atmospheric parameters). A main result of this study was that GRACE satisfactorily detected the seasonal water storage changes over whole West Africa and their inter-annual variability over the Sahel. The models, on the other hand, could not adequately reproduce the strong inter-annual variability, and showed large deficiencies during the dry season. The seasonal cycles estimated by GRACE and the ALMIP models showed some phase difference consistent with the findings of *Schmidt et al.* [2008] for global models. *Grippa et al.* [2011] attributed these discrepancies to mismodeling issues, like approximations in the horizontal transport through the rivers and neglect of slow water reservoir effects. Besides, the GRACE products and model representativity are not completely equivalent, as GRACE accounts for total terrestrial water storage including aquifers and surface water contained in the riverbeds and floodplains, which are usually not present in land surface models.

[8] The present study compares the results from the CNRS/GRGS GRACE product, loading model simulations accounting for continental water storage, atmospheric loading and nontidal oceanic loading, and GPS ground deformations. The data set is presented below in section 2. Section 3 compares the GPS- and GRACE-derived ground deformation estimates with the loading model simulations and determines to which extent the GPS may be used to improve our knowledge of the continental water storage cycle in West Africa. Section 4 investigates the potential geophysical origin of a transient signal detected in the GPS position time series, possibly related to nonloading soil expansion. The results are summarized and discussed in section 5.

2. Data and Methods

2.1. GPS

[9] Six of the permanent GPS stations used in this study were initially installed within the framework of AMMA [*Bock et al.*, 2008]. They contribute now to the GHYRAF project [*Hinderer et al.*, 2009]. Three of them have been running continuously since mid-2005 (Niamey (NIAM), Djougou (DJOU) and Gao (GAO1)) and three others (Ouagadougou (OUAG), Tamale (TAMA) and Timbuktu (TOMB)) since mid-2006. To guarantee the required mechanical stability, the antennas were mounted on the top of reinforced concrete pillars 1 m in height set above a buried concrete foundation of 1 m^3. The TAMP GPS station is a permanent station operating at the geophysical observatory of Tamanrasset by the CRAAG (Centre de Recherches en Astronomie, Astrophysique et Géophysique, Alger). These seven sites sample a range of climates from the arid Sahara desert (TAMP records only 20 mm of rainfall per year) to the moist Sudano-Guinean region (DJOU reaches 1100 mm/yr of precipitation [*L'Hote and Mahé*, 1996]). The other stations used in this study are part of the International GNSS Service (IGS) network [*Dow et al.*, 2009].

2.1.1. GPS Data Analysis

[10] The GPS Receiver-Independent Exchange (RINEX) data from the AMMA stations were processed by the University of La Rochelle Analysis Center Consortium (ULR) from mid-2005 to the end of 2008. They are part of the fourth ULR solution (ULR4 hereafter), which is freely available at http://www.sonel.org/-GPS-Solutions-.html [*Santamaría-Gómez et al.*, 2011]. The ULR4 solution is based on a homogeneous state-of-the-art reprocessing using the GAMIT 10.34 release [*Herring et al.*, 2008]. It covers a global network of 316 stations and a period from 1996 to the end of 2008. To reduce the processing overload, the network was split into several subnetworks. Six common IGS reference frame stations were included in every subnetwork to allow the combination of the station positions for each subnetwork (see subsection 2.1.2). The design of the network and the choice of the six common stations were optimized daily, depending on the stations actually available. Satellite orbit parameters were adjusted during the reprocessing, starting with the IGS precise orbits as a priori values. Absolute antenna phase calibration models were applied [*Schmid et al.*, 2007]. Atmospheric gradients and zenith tropospheric delays (ZTDs) were adjusted every 24 h and 2 h, respectively, using the VMF1 mapping function [*Boehm et al.*, 2006; *Kouba*, 2008]. A priori ZTDs were derived from the ECMWF model [*Boehm et al.*, 2006] and the cutoff angle was fixed to 10°. Ocean tide loading effects were corrected using the FES2004 model [*Lyard et al.*, 2006]. Neither higher ionospheric effects nor atmospheric loading (tidal and nontidal) and nontidal ocean loading were corrected for. A more complete description of this GPS analysis strategy can be found in *Santamaría-Gómez et al.* [2011, 2012].

[11] The atmospheric pressure tidal loading effects over West Africa are at the level of 1 mm and 1.1 mm for diurnal and semidiurnal components, respectively [*Bock et al.*, 2008] based on model simulations from *Petrov and Boy* [2004]. This loading component is thus small and the aliasing effect resulting from not correcting it manifests as spurious signals at periods close to the GPS draconitic annual and semiannual periods of 351 and 175 days, respectively [*Tregoning and Watson*, 2009, 2011]. The amplitude of the semiannual draconitic period is latitude dependent and reaches a maximum at the level of 0.2 mm at latitudes between 20 and 25° in both hemispheres. Hence, we neglected the tidal atmospheric loading effect in our analysis.

[12] Nontidal atmospheric loading effects, on the other hand, were shown to impact the vertical component of GPS stations at the 1 to 2 mm level [*Tregoning and Watson*, 2009; *Dach et al.*, 2011]. Oceanic loading effects could also reach the mm level in the vertical component at coastal sites [*Williams and Penna*, 2011]. As the aim of this study was to examine whether the GPS was able to detect various loading effects at seasonal timescales, we chose not to correct the nontidal atmospheric and oceanic loadings, neither at the observation level, nor in the solution. However, in this study, we expected very small crustal deformations (well below 1 mm) induced by nontidal oceanic loading at the sites of interest. Higher-order ionospheric effects were not corrected for since no appropriate model was available at the time of the reprocessing. However, as shown by recent studies [*Hernandez-Pajares et al.*, 2007; *Petrie et al.*, 2010], the impact of neglecting second- and third-order ionospheric refraction terms on the mean (long-term) station positions near the Equator is at the sub-mm level with a quasi-annual oscillation in the North component of less than 1 mm. The amplitude also depends on the solar activity. For the main period of interest here (2005–2008), the ionospheric activity was at a minimum. Therefore, we neglected these effects which did not impact our GPS station positions significantly.

2.1.2. Deformation Time Series

[13] We combined station positions from each subnetwork into daily network solutions and then we stacked them into weekly station positions using the GLOBK software [*Herring et al.*, 2008]. These loose (frame-free) weekly station positions were transformed and stacked into a long-term frame solution. We aligned this long-term solution to the ITRF2005 [*Altamimi et al.*, 2007] using the CATREF software [*Altamimi et al.*, 2007] and minimal constraints over the transformation parameters on a selected set of 68 IGS reference frame stations. The scale parameter between the weekly and long-term frames was not estimated as it has been shown to absorb partly the deformation due to surface loadings (especially the atmospheric loading) [*Tregoning and van Dam*, 2005; *Collilieux et al.*, 2011a]. From the stacking of the weekly station positions, the mean station position at a reference epoch, the linear trend and any offset due to earthquakes and equipment changes were estimated for each station. Then, we retrieved the nonlinear station displacements as the residuals of the weekly combined solution with respect to this model.

[14] The Center-of-Mass (CM) of the Earth's system is defined as the center of mass of the solid Earth and its fluid envelope. In GPS processing, estimating simultaneously satellite orbits and loosely constrained station positions results in station coordinates theoretically expressed in the CM frame. However, the terrestrial frame origin is in practice not well determined from GPS data alone (at least it is less precise than derived from SLR data [*Blewitt*, 2003; *Collilieux et al.*, 2011a]). Our transformed GPS solution was in ITRF2005. The origin of this frame is consistent with the CM on the secular timescale, but fixed (in terms of motion) to the geometric Center-of-Figure (CF) at seasonal and shorter timescales [*Dong et al.*, 2003]. Short-term network translations from a global and well-distributed geodetic network like the ITRF2005 ideally approximate the CF-CM motion at the level of 0.2 to 0.3 mm RMS in X, Y, and Z [*Collilieux et al.*, 2011a]. We thus considered with a good approximation that our GPS station position residuals were expressed in the CF frame.

2.1.3. Quality of the GPS Solution in Africa

[15] The precision of the GPS positions and velocities from the ULR4 solution has been assessed in the work of *Santamaría-Gómez et al.* [2011, 2012] and proved to be comparable to the IGS station used in the ITRF2005 [*Altamimi and Collilieux*, 2009]. More recently, the ULR4 solution was included in the first IGS reprocessing campaign and showed to be as accurate as the other IGS Analysis Center solutions [*Ferland*, 2010]. The weekly position repeatability, computed as the weighted RMS of the daily station position residuals with respect to the weekly combined position, was actually between 1 and 3 mm in the horizontal component and between 4 and 6 mm in the vertical component.

[16] Figure 2a focuses on the vertical component for the African GPS stations used in this work. The median repeatability at the African stations ranges between 2.5 and 4.5 mm and is decreasing with latitude. This level of repeatability is comparable to that of ONSA (Onsala, Sweden) or GODE (Greenbelt, USA), which are considered as high-quality IGS stations and are part of the IGS Reference Frame (ONSA and GODE have a repeatability of 3.8 mm and 3.2 mm, respectively in the ULR4 solution). The time series of the one month running average of repeatability is presented in Figure 2b for stations DJOU, GAO1 and NIAM. There is a strong semiannual modulation in the repeatability which appears to be correlated with the monsoon seasonal cycle. The values are below 2–3 mm from October to April, during the dry season, and above 4.5–6 mm from June to August, during the wet season when the troposphere is more active (frequent passage of mesoscale convective systems and easterly waves, with characteristic periods smaller than one week). The noise level in the GPS position time series increases also during the wet season, and this may be explained either by rapid station vertical motions (with subweekly period) or by reduced positioning precision due to modeling deficiencies although state-of-the-art modeling was used here (e.g. VMF1 mapping functions and ECMWF derived a priori ZTD values). To mitigate the impact of high tropospheric activity and mismodeling on the GPS vertical component, we used only weekly position estimates in the following. This sampling period is well adapted to represent subseasonal variability.

2.2. GRACE Analysis

[17] We first transformed GRACE gravity field time variations into surface mass variations [*Wahr et al.*, 1998] and

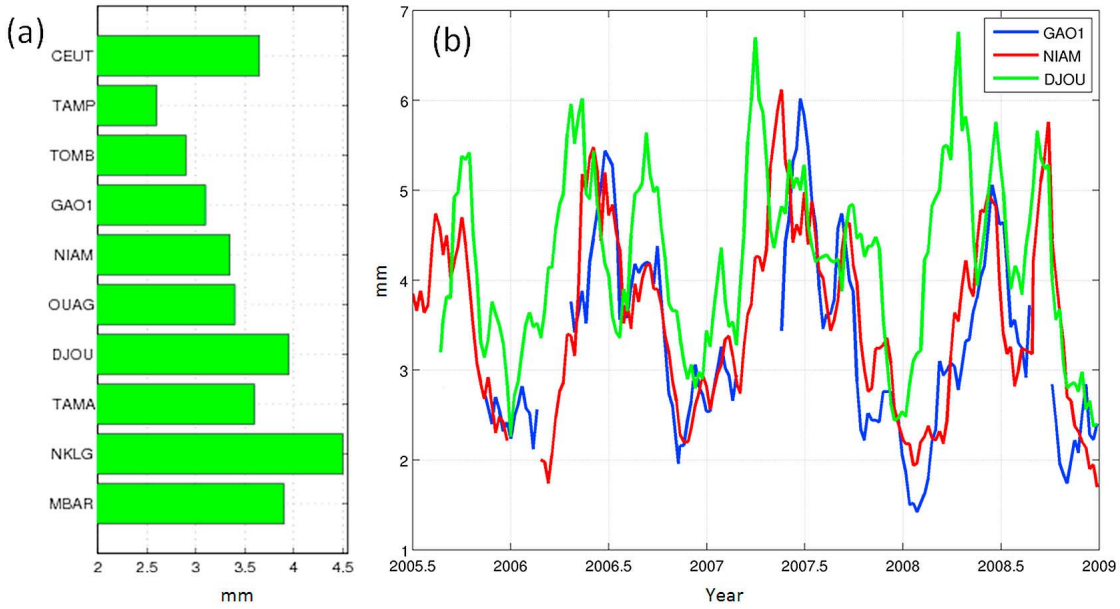

Figure 2. (a) Median values of the repeatability in the vertical component of African stations ordered by decreasing latitude from CEUT (Spain) to MBAR (Uganda). Repeatability is computed as the weighted RMS of the daily station height residuals with respect to the weekly combined height. The median is taken over the whole period of observations. (b) Time series of repeatability, smoothed with a one month moving average, for three stations: GAO1 (blue curve), NIAM (red curve) and DJOU (green curve).

we computed then ground deformations using load Love numbers corresponding to an elastic Earth model [*Farrell*, 1972]. To remain consistent with the GPS position estimates, the loading contributions from hydrology, oceans and the atmosphere, and the geocenter motion (translation between the CF-frame and the CM-frame) must be properly taken into account.

2.2.1. Time-Variable Gravity Data

[18] We used the 10 day GRACE gravity solution field from release 2 of the CNES/GRGS product up to degree and order 50 [*Bruinsma et al.*, 2010]. At seasonal timescale, this solution is well consistent with the other solutions, even if exhibiting slightly higher-than-average annual variation amplitudes [*Grippa et al.*, 2011; *Hinderer et al.*, 2011]. The GRGS product models the contributions of the atmospheric surface pressure variations and of the barotropic ocean response to wind and pressure forcing using the 6 hour grids from the ECMWF [*Uppala et al.*, 2005] and MOG2D-G [*Carrère and Lyard*, 2003] models, respectively. These effects are removed from the Stokes coefficients of the time-variable gravity potential. Due to model uncertainties and unmodeled high-frequency signals, the GRACE gravity potential products exhibit north south oriented systematic artifacts so-called "stripe noise" [*Panet et al.*, 2010], which is usually filtered out using a low-pass spatial filter [*King et al.*, 2006]. However, the later conversion of mass distribution into ground deformation results in a low-pass filtering which removes most of the stripe noise. For example, we tested the use of a 500 km Gaussian filter and found differences in vertical displacements not larger than ± 1 mm at the African GPS stations.

[19] In a first step we compared GPS estimates with GRACE and loading models. This required providing consistent estimates of the total deformation due to the atmosphere, ocean and soil moisture. To obtain GRACE gravity time variations consistent with the GPS deformations, atmospheric loading effects (tidal and nontidal) and nontidal barotropic ocean response effects must be added back into the GRACE products [e.g., *Tregoning et al.*, 2009]. To do so, we used the above-mentioned ECMWF and MOG2D-G models (the so-called GRACE de-aliasing products) to reinsert these loading effects into the GRACE gravity potential coefficients before computing the equivalent mass anomalies following the procedure of *Wahr et al.* [1998].

2.2.2. Ground Deformations

[20] We computed the 3-D deformations caused by the surface density anomaly field derived from GRACE at every GPS station of our network using load Love numbers and following the procedure of *Farrell* [1972]. These Love numbers were deduced from the Preliminary Reference Earth Model (PREM) [*Dziewonski and Anderson*, 1981], which accounts for the Earth's sphericity and radial heterogeneity but neglects ellipticity and lateral heterogeneity. The effect of the ellipticity on degree 2 and degree 3 load Love numbers is close to 1% [*Métivier et al.*, 2005]. As West Africa is located at low latitudes, we considered that this effect was negligible for the estimation of the deformations.

[21] Since GRACE does not observe degree-1 mass or deformation, a degree-1 estimate must be inserted in the GRACE product for the computed deformation field to be complete. Therefore we did not use the degree-1 coefficients provided in the CNES/GRGS release 2 solution. Instead, we used the degree-1 model derived from the long term components provided by *Munekane* [2007] and from the seasonal variations provided by *Wu et al.* [2010]. This model was produced from IGS reprocessed GPS solutions, ocean bottom pressure observations and GRACE data [*Wu et al.*, 2010]. We computed the degree-1 deformation over the period of

study using the corresponding load Love number in the CF frame [*Blewitt*, 2003] and added it to the GRACE deformation estimate to be consistent with the GPS estimates in the CF frame.

[22] Our GRACE surface deformation estimates contain thus signals related to subsurface water mass redistribution and atmospheric pressure variations over land (termed hydrologic and atmospheric loadings, respectively), effects of baroclinic ocean response, and effects of secular mass changes in the solid Earth (e.g. due to glacial isostatic adjustment) and in the subsurface layer (e.g. due to polar ice and trend in hydrology).

[23] We finally obtained consistent GRACE and GPS deformation estimates even if their agreement is inevitably limited by the fact that GPS deformations give local information whereas GRACE estimates are representative of a spatial scale of ~400 km. For this reason, results from both techniques should be interpreted carefully, not excluding the possibility for observing local hydro-geological signals in the GPS data. On the other hand, previous work demonstrated that regional-scale loading signals are well captured by both techniques [e.g., *Tregoning et al.*, 2009].

2.3. Loading Models

[24] We computed ground deformations due to hydrological, atmospheric or nontidal ocean loading using various model outputs. Deformations from hydrological origin were estimated using the Global Land Data Assimilation System (GLDAS) [*Rodell et al.*, 2004] driving the Noah land surface model [*Ek et al.*, 2003; *Chen et al.*, 1996]. The model was used with a $0.25° \times 0.25°$ spatial resolution and a 3 hour time step, and was forced either by the Climate Prediction Center operational global 2.5°, 5 day, Merged Analysis of Precipitation (CMAP) [*Xie et al.*, 2003] or by the NASA-NASDA Tropical Rainfall Measuring Mission (TRMM) [*Huffman et al.*, 1997] precipitation fields. The GLDAS/Noah model has been widely used in the last years. *Grippa et al.* [2011, Figures 7 and 8a] showed that it was very consistent with 8 other models over West Africa and Sahel, both in terms of spatial distribution and of seasonal variations.

[25] Atmospheric loading effects were derived from the ECMWF reanalysis ERA-Interim [*Dee et al.*, 2011]. The surface pressure field in the reanalysis is available every six hours on a $0.75° \times 0.75°$ horizontal grid over the orographic surface used in the model. The model surface differs from the real topography but the errors introduced by differences in West Africa are very small. Deformations due to the loading effect of the nontidal oceanic component (barotropic and circulation terms) were computed using the MOG-2D ocean model [*Carrère and Lyard*, 2003]. We directly expressed all the loading model deformation outputs with respect to the CF frame to be consistent with the GPS deformations.

3. Deformation Analysis

3.1. Example of the Niamey Station

[26] Niamey (13.5°N, 2.18°E) is located in the southwest of the Republic of Niger, in a region representative of the southern Sahel. It receives a total annual amount of precipitation of 565 mm (average estimate from Global Precipitation Climatology Project (GPCP) [*Huffman et al.*, 1997], over the 2002–2008 period) during the monsoon season, between June and September. The inter-annual variability in precipitation at Niamey is large over the period, with low rates in 2002, 2004, 2006 and 2008, and high rates for the other three years (Figure 3a). According to the GLDAS model and GRACE observations, the seasonal variation in soil moisture induced by the monsoonal rainfall reaches its maximum in September–October and its minimum in May–June (Figure 3b). The lag of the response of the soil moisture maximum to the precipitation maximum is due to the fact that precipitation is a flux and soil moisture is an integrative quantity. The modeled hydrological loading signal induced by the soil moisture anomaly consists in a maximum downward motion in September–October and a maximum uplift in May–June. Its inter-annual variability is clearly related to the variability in precipitation (Figure 3b). The hydrological loading signal as represented by GLDAS is very smooth compared to the atmospheric loading and its average peak-to-peak annual amplitude is 10 mm. The modeled atmospheric loading shows a deformation up to 5 mm with an annual periodicity due to the seasonal displacement of the Saharan Heat Low [*Lavaysse et al.*, 2009]. Its more rapid variations are due to the passage of synoptic-scale weather systems. For the comparison with the estimated GPS ground deformation (Figure 3c–3e), we added the nontidal contributions from the atmosphere and the ocean to the hydrological loading.

[27] The comparison of the vertical deformation estimated by the GPS and GRACE analyses with the model estimates reveals a quite good agreement (Figure 3c). The seasonal signal due to hydrological loading is the predominant process at Niamey. The linear correlation coefficient between the sum of models and GRACE is $r = 0.93$. It is lower ($r = 0.70$) between GPS and either GRACE or the models but this level of correlation still compares well to the best results reported by *Tregoning et al.* [2009], and *Tesmer et al.* [2011]. The root mean square (RMS) of the difference between the sum of models and GRACE is 1.9 mm (3.1 mm between GPS and GRACE and 3.5 mm between GPS and the models). As observed in Niamey in Figure 3, and at the other stations in Figures 4–6, the difference between the models and GRACE is partly due to the underestimation of the annual amplitude of the hydrological signal in the GLDAS model (Figure 1). This was already observed in previous studies [see, e.g., *Ramillien et al.*, 2005; *Schmidt et al.*, 2008]. The difference between GPS and the two other estimates is mainly due to an additional signal in the GPS time series at the end of the year (Figure 3c). It appears as an oscillation which superimposes on the quite monotonous uplift observed in the GRACE estimates from October to May. This oscillation indicates a secondary maximum uplift in December and a secondary maximum subsidence in February. We compared the vertical deformations observed at Niamey with those of other stations in section 3.2.

[28] The horizontal components (Figures 3d and 3e) show also a clear seasonal variation but of much smaller amplitude (2 mm peak-to-peak for the north (N) component estimated by GRACE or the models, and 1 mm for the east (E) component). Again, the deformation estimated by GPS shows an additional signal that appears rather random but its extrema are in phase with the extrema observed in the up (U) component. Hence it is likely that GPS senses local deformations that are neither represented in the GRACE nor in the model

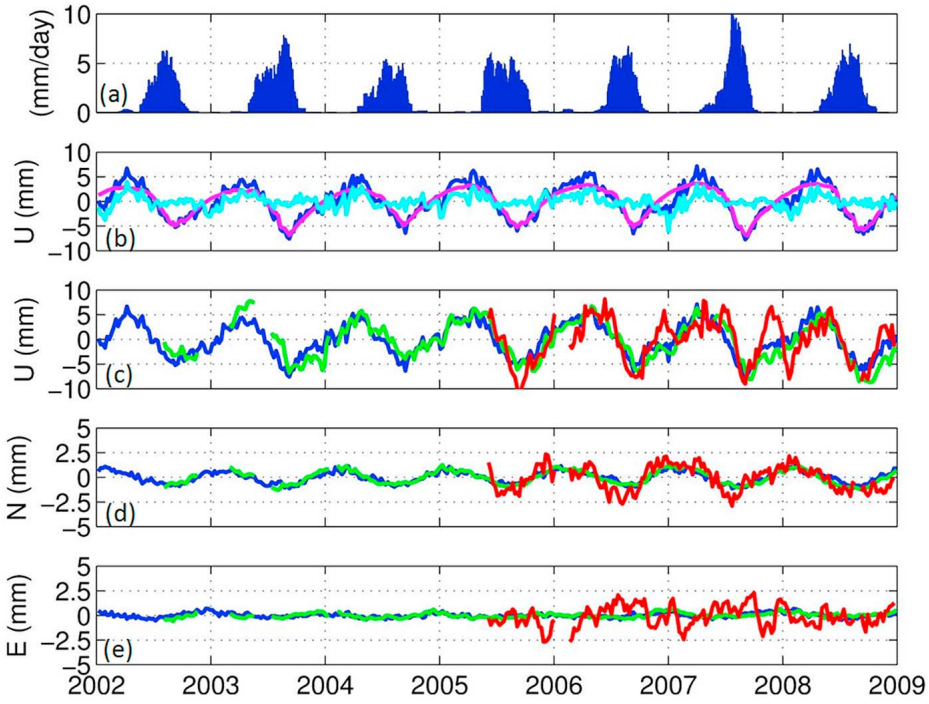

Figure 3. Time series of (a) GPCP precipitation at Niamey (mm/day); (b) modeled loadings: hydrology from GLDAS (magenta), atmosphere from ECMWF + ocean from MOG-2D (cyan) and sum of models (blue); (c) detrended component of vertical deformation from GPS (red), the sum of models (blue) and GRACE (green); (d, e) similar to Figure 3c but for N and E deformation components, respectively. The GPCP data are smoothed with a 30 day running mean and the other data are smoothed with a 10 day running mean and re-sampled at a 10 day interval.

estimates. Since the monsoon system has a strong latitudinal structure, the E component of deformation is very small and is not further discussed. At NIAM, the modeled N component resulting from the combination of hydrologic and atmospheric loadings shows similar annual amplitude but a dephasing of 4–5 months between their subsidence maxima (not shown). This delay corresponds to the time lag between the passage of the Heat Low depression (April–May) and the maximum of the soil moisture anomaly (September). The N component of the hydrologic loading points actually toward the barycenter of the soil moisture anomaly which is located around 10°N in August–September (Figure 1a). The inspection of the N component for the other AMMA stations confirms this point (e.g. the amplitude of the hydrologic anomaly is almost zero at DJOU). The phase of the atmospheric part is quite different between the southern sites (DJOU and TAMA) and the Sahelian sites (NIAM, GAO1, TOMB) due to the different influence of high and low surface pressure systems over the region (e.g. in July a large pressure gradient is pointing southward, whereas in January it is pointing northward).

3.2. Regional Analysis of the Vertical Deformation

[29] The seasonal evolution of the vertical deformation observed at NIAM is quite well repeated at the other AMMA sites (Figure 4). The six AMMA sites show a strong seasonal oscillation with a minimum in the U component (subsidence) in September and a maximum (uplift) in May. This oscillation reflects a strong regional loading signal, with a peak-to-peak amplitude comprised between 10 mm at TOMB and GAO1 and 15 mm at TAMA and DJOU, as estimated by GRACE and GPS. It is clearly induced by the monsoon system and is primarily due to its hydrologic loading component. The annual harmonic of the hydrologic loading actually dominates the ocean+atmosphere loadings at the six AMMA sites and increases from north to south (Figure 5a). The combined ocean+atmosphere loadings, on the other hand, increase from south to north with a maximum at TOMB due to the proximity of the Heat Low depression in summer.

[30] Figure 4 shows that the three data sets agree quite well at the six AMMA sites. The average linear correlation coefficient between GRACE and the models is r = 0.93, and r = 0.66 between GRACE and GPS. At the four other sites located outside of the monsoon area, the agreement is less good (r = 0.78 between GRACE and the models and 0.18 between GRACE and GPS), but the deformation signal is also much smaller. Especially for GPS it is at the limit of accuracy of the technique. The comparison between GPS and the models yields slightly better results than between GPS and GRACE (r = 0.70 at the six AMMA sites and 0.27 at the four other sites), suggesting that GPS and model estimates contain local loading deformations that are not well resolved by GRACE. The RMS difference between GRACE and the models is 1.9 mm on average over the AMMA sites. It is 3.6 mm between GRACE and GPS and.3.2 mm between GPS and the models. Besides the good agreement between

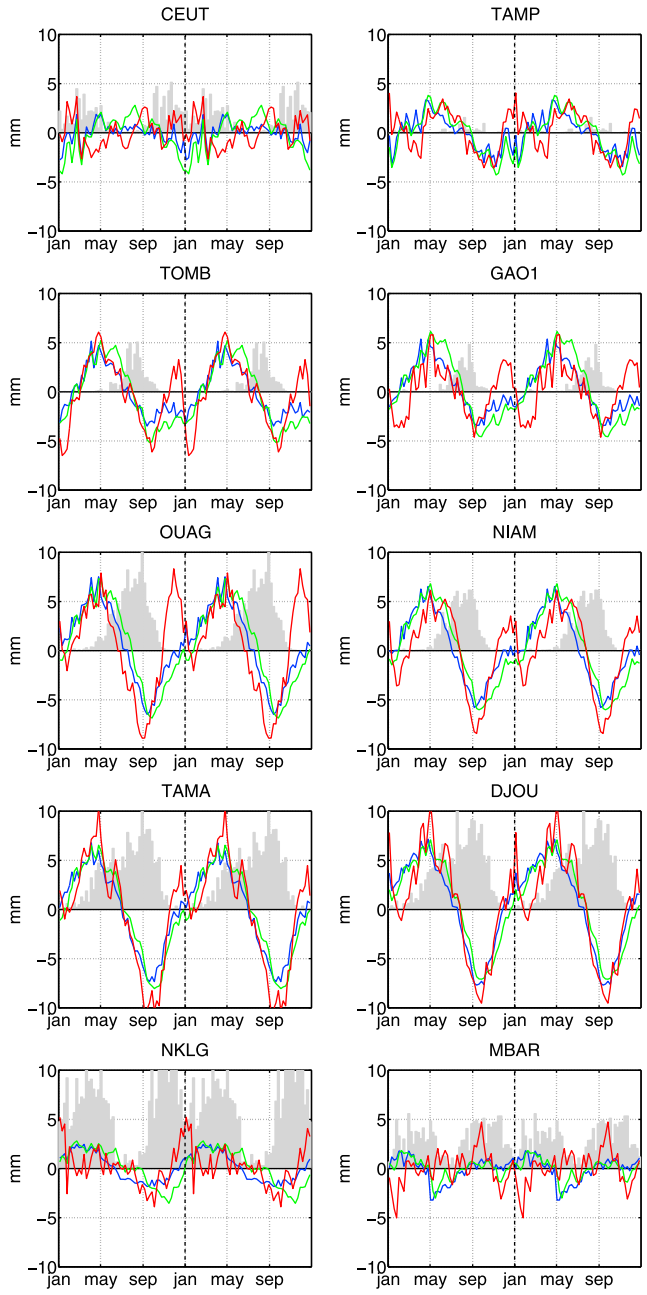

Figure 4. Mean annual signals of vertical displacements derived from the GLDAS+ECMWF+MOG2D models (blue), GRACE (green), and GPS (red) in mm. The gray shaded background shows the mean annual precipitation from GPCP satellite product. The means are computed over the 2005–2008 period. The signals are repeated over two years and the dotted vertical line indicates the change of year.

all three data sets, a striking feature is the additional signal (oscillation) in the GPS vertical deformation already noticed above (Figure 3). This oscillation is actually present and nearly in phase in the GPS estimates from all six AMMA sites. It is especially strong at OUAG, NIAM, GAO1, and TOMB. Whether this additional signal reflects a real deformation of the surface or stems from an artifact of the GPS measurement or data processing is an intriguing question that we try to elucidate in sub-section 3.3.

[31] Figure 5a shows that the annual harmonics of the GPS deformation is in quite good agreement with the sum of models, but both GPS and the models underestimate slightly the GRACE estimates. For the semiannual harmonic (Figure 5b), GRACE and the models agree much better, but the GPS deformation is larger by a factor of 2 to3. This fact reflects the presence of the additional signal in the GPS estimates (Figure 4) which has a duration of approximately 6 months and induces thus a strong semiannual harmonic in the GPS spectrum. Figure 5b reveals also a significant semiannual harmonic at TAMP and NKLG. Figure 4 suggests that the GPS vertical deformation estimates at both sites contain a similar additional signal. Both sites are actually close to the West African Monsoon region and may be under the influence of similar geophysical phenomena. At the other two sites (CEUT and MBAR), and also at most of the sites of the global GPS network (not shown), we do not observe this signal.

[32] Table 1 reports the linear correlation coefficient between the vertical components of the GPS residual signals (GPS minus GRACE), at the sites where it is significant. Clearly, all the stations located in West Africa have correlated residual signals. This is usually not the case for stations located in other regions at similar or shorter inter-site distances (not shown). Hence, the GPS residual signal observed at the AMMA stations is really specific to the study area and we consider seriously the possibility that it is a real deformation linked to the monsoon system.

3.3. Is the Additional Signal in the GPS Vertical Deformation an Artifact?

[33] The ground deformation represented by GRACE and the models is essentially due to regional-scale loadings. These two estimates are in good agreement, and the model products used in this study are consistent with independent model estimates provided by T. Van Dam (University of Luxembourg). We can assume that the additional signal seen in the GPS vertical deformation is probably not a loading effect, at least at the regional scale. A cautious approach is to investigate whether this signal can be due to error sources specific to the GPS technique and/or potential GPS data processing artifacts.

[34] Given that the additional signal that we are tracking expresses strongly at the semiannual timescale (Figure 5), it can either result from the direct mapping of a spurious semiannual signal or from the aliasing of an unmodeled subdiurnal signal [*Penna and Stewart*, 2003; *Penna et al.*, 2007; *King et al.*, 2008]. However, since we used reprocessed GPS data which were analyzed with the most recent modeling approaches (mapping functions, a priori zenith hydrostatic delays, ocean tide loading and EOPs) and given that unmodeled effects such as stemming from higher order ionospheric refraction and tidal atmospheric loadings are expected to be at the 1 mm level or below (Section 2.1), we are confident in the GPS analyses used in this study. Other errors that may remain in our GPS analyses are: mismodeled tropospheric delay variations, unmodeled near-field antenna effects (multipath and antenna phase center variations),

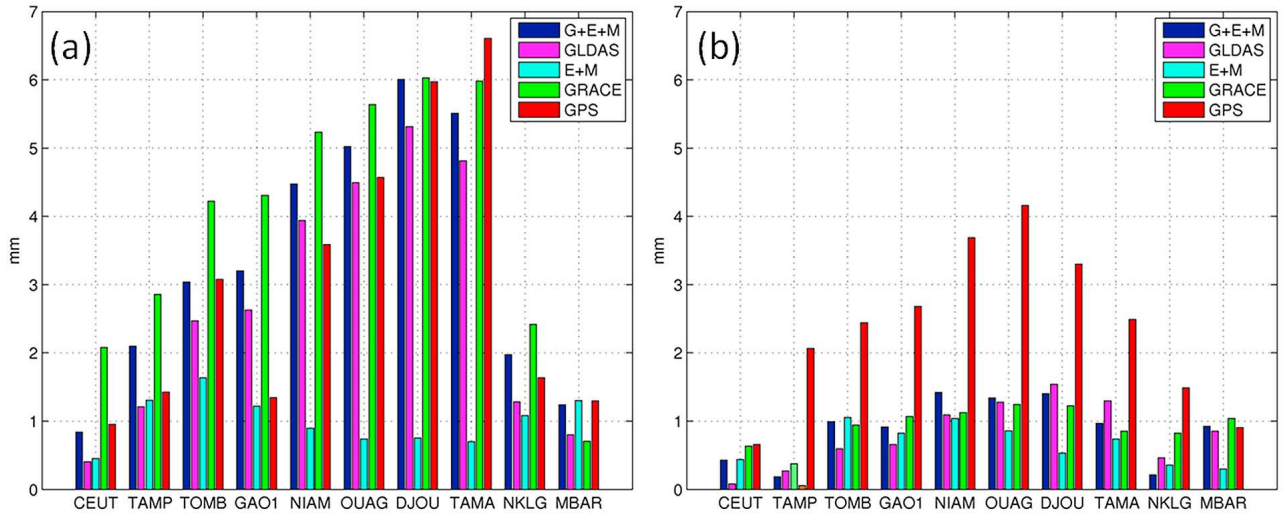

Figure 5. (a) Annual amplitudes and (b) semiannual amplitudes of the vertical deformation time series for 10 African stations and each data set. Stations are ordered by decreasing latitude from CEUT (Spain) to MBAR (Uganda).

mismodeled ocean loading, and unmodeled thermal expansion of monuments and nearby bedrock.

[35] In West Africa, fluctuations in the atmospheric moisture content cover a broad range of timescales [*Bock et al.*, 2008] and may produce both direct and aliased tropospheric errors. As an estimate of the uncertainty due to the tropospheric modeling, we can refer to the results of *Tregoning and Watson* [2009, Figure 7], who found differences in the annual and semiannual signals for the vertical component of less than 0.5 mm for most sites, and extreme values below 1.6 mm at a few high-latitude sites.

[36] Seasonal changes in the surface and vegetation properties as documented by *Descroix et al.* [2009] and *Favreau et al.* [2009] may also induce changes in multipaths. The impact of multipaths was recently reassessed by *King and Watson* [2010], on the basis of simulations. They evidenced time-variable errors in station coordinates with spectral peaks at the harmonics of the draconitic period for the GPS satellites (∼351 days) up to order 20 and more, but their simulations did not reveal a preferential error at semiannual period. Changes in the observing geometry (e.g. changes in the GPS satellite constellation or in site specific obstructions) were shown to modulate significantly seasonal and longer fluctuations, while fixing ambiguities was shown to minimize these effects.

[37] Antenna phase center variations are thought to produce similar effects as multipath [*King and Watson*, 2010]. All these error sources taken together likely produce an increase of scatter in the station positions and phase residuals during the wet season. This is indeed what we observe both in the station heights (Figure 2b) and RMS phase residuals (not shown). However, these extra error sources cannot explain the near one cm additional signal that we observe during the dry season.

[38] Another possible error source might be the aliasing of loading signals on the GPS frame transformation parameters as discussed by *Collilieux et al.* [2011b], but it results primarily into a spurious annual signal in the transformation parameters and in the GPS coordinate time series.

[39] *Dong et al.* [2002], *Yan et al.* [2009], and *Tesmer et al.* [2011] discussed also the possible impact of thermal expansion of monuments and nearby bedrock, but these authors could not conclude on a clear correlation with spurious (not due to loading) GPS residuals.

[40] The large semiannual signal may also be a manifestation of the draconitic frequencies highlighted by *Ray et al.* [2008]. Figure 6a presents the spectra of the vertical deformations as represented in the three products, stacked over the six AMMA GPS stations. The spectrum of the GPS deformation shows annual and semiannual peaks, as well as peaks

Table 1. Linear Correlation Coefficients Between the GPS Residual Signals (GPS Minus GRACE) From Pairs of Stations[a]

Station	CEUT	TAMP	TOMB	GAO1	NIAM	OUAG	DJOU	TAMA	NKLG	MBAR
CEUT	1	0.41**			−0.10				−0.06	−0.31**
TAMP		1	0.15	0.20*	**0.60****	−0.05	**0.60****		0.44**	−0.18*
TOMB			1	**0.64****	0.49**	**0.56****	0.48**	**0.56****	0.12	−0.14
GAO1				1	**0.63****	**0.74****	0.47**	0.45**	0.22**	0.14
NIAM					1	0.49**	**0.65****	0.36**	**0.52****	0.03
OUAG						1	0.30**	0.42**	0.27**	−0.23**
DJOU							1	**0.55****	0.40**	0.07
TAMA								1	0.13	−0.11
NKLG									1	−0.10
MBAR										1

[a]Statistical correlation confidence test: (*) 10% and (**) 5%. Values larger than 0.50 are bold.

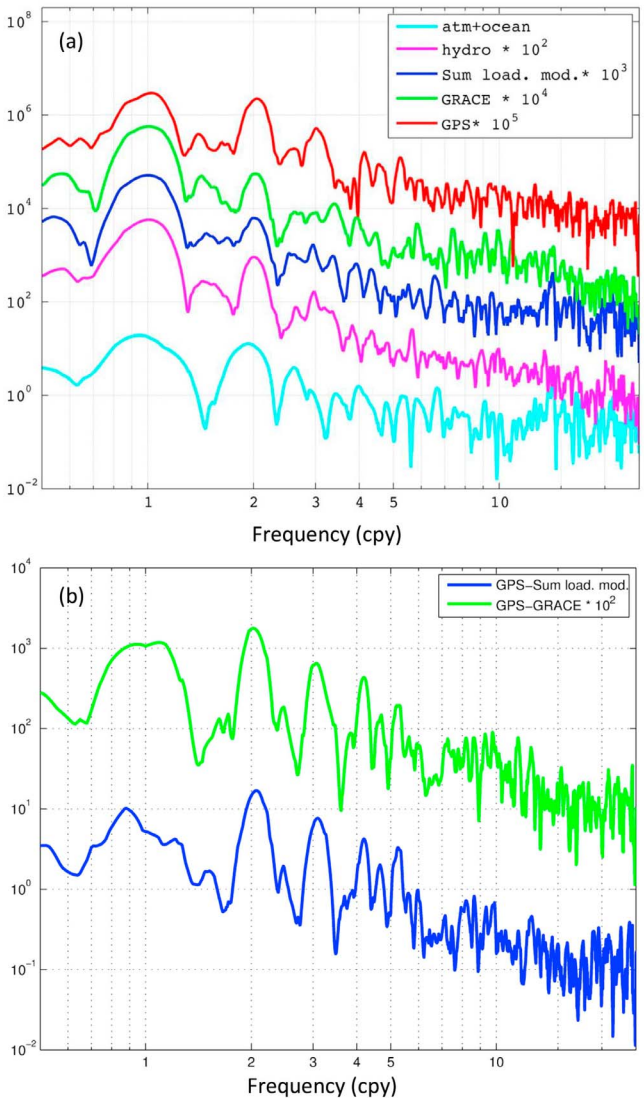

Figure 6. Stacked Lomb-Scargle normalized periodograms [*Press et al.*, 1992] of the vertical deformations estimated at the six AMMA GPS stations by: (i) ocean and atmosphere models (MOG2D and ECMWF models – cyan curve), (ii) hydrologic model (GLDAS model – magenta curve), (iii) the sum of models (blue curve), (iv) GRACE (green curve), and (v) GPS height residuals (red curve). All the data sets are reduced to a common temporal sampling over the 2005–2008 period. The unit of the x-axis is number of cycles per year (cpy).

at higher frequencies (e.g. at 3.1, 4.2, and 5.2 cpy) that cannot be clearly identified in the GRACE data or in the geophysical models and may thus suggest the presence of draconitic signals. This is also reflected in Figure 6b showing the spectra of differences (GPS minus sum of models or GRACE). However, the harmonic comb seen in Figure 6b is not surprising and corresponds exactly to what one can expect from a transient oscillation of 175 day duration and 351 day periodicity which is more or less the signature of our additional signal. Hence, though the additional signal has a spectral signature very similar to what is usually interpreted as draconitic signal, its amplitude is too large to be assimilated to a spurious signal resulting from any of the known error sources in GPS analysis.

4. A Possible Geophysical Origin of the Additional GPS Deformation Signal

[41] In this section we investigate the possible link between the additional deformation signal seen in the GPS solution and local geophysical processes inducing variations in the surface water budget. First, we present the hydro-geological background necessary to understand the main processes affecting the three sites located along the Niger River (Timbuktu, Gao, and Niamey). Then we use complementary available data sets to highlight the coincidence between surface water parameters and residual GPS signal at these sites as well as at Ouagadougou. Because of the lack of colocated hydrological observations at the other two sites (Djougou and Tamale), they are not further discussed here. These are also the sites where the residual signals are the smallest.

4.1. Hydro-geological Background

[42] The six AMMA GPS stations lie on various hydrogeologic provinces (Figure 7). Niamey [*Greigert*, 1968] and Timbuktu [*Saad*, 1971] are located on the Azawad and Iullemenden sedimentary basins which contain continental sediments (mainly sandstones, siltstones and clays) belonging to the Continental Intercalaire and Continental Terminal series formations. These formations are locally covered by quaternary aeolian deposits. At present time, recharge of the aquifer occurs there mainly from ponds located in topographic lows, which are filled by runoff during heavy rainfall events. Recharge by the Niger River is negligible a few km away from the river channel [*Desconnets et al.*, 1997; *Jacks and Traoré*, 2008]. By contrast Ouagadougou, Djougou, and Tamale are located on weathered basement, consisting in metamorphic rocks, and granite overlaid by laterites resulting from weathering of this basement in a humid tropical climate. Laterites contain iron and aluminum oxides, but also clay mineral produced in the early stages of weathering [*Tardy*, 1997]. In these areas, recharge of the aquifer has been shown to occur mainly by diffuse infiltration of rainwater through the laterite layer [*Yameogo*, 2008; *Seguis et al.*, 2011].

[43] West Africa hosts three large watersheds supplying the Niger, the Senegal and the Volta rivers. The Niger watershed (Figure 7) is the fourth biggest in Africa; it extends over more than 2×10^6 km^2. The source of the Niger is located in the Guinean highlands near the border between Sierra Leone and Guinea. The Niger River runs northeastward from there into the Sahel, until it reaches Timbuktu and then turns southeastward, passing near Gao and Niamey and finally exits into the Ocean in the south of Nigeria. Though the Sahel is usually considered as an endorheic area at large, our three Sahelian stations are located in the Niger River active watershed [*Descroix et al.*, 2009]. Because of the large north south gradient in precipitation, most of the water transported northward by the Niger River to the Sahel is not of local origin but is supplied by the first drainage basin of the Upper Niger indicated as area I in Figure 7. The high amount of upstream water collected during the rainy season produces a flood wave, called the "Guinean flood" or also the "black flood", which peaks during the first week of September at Bamako. The flood wave arrives at Timbuktu several weeks

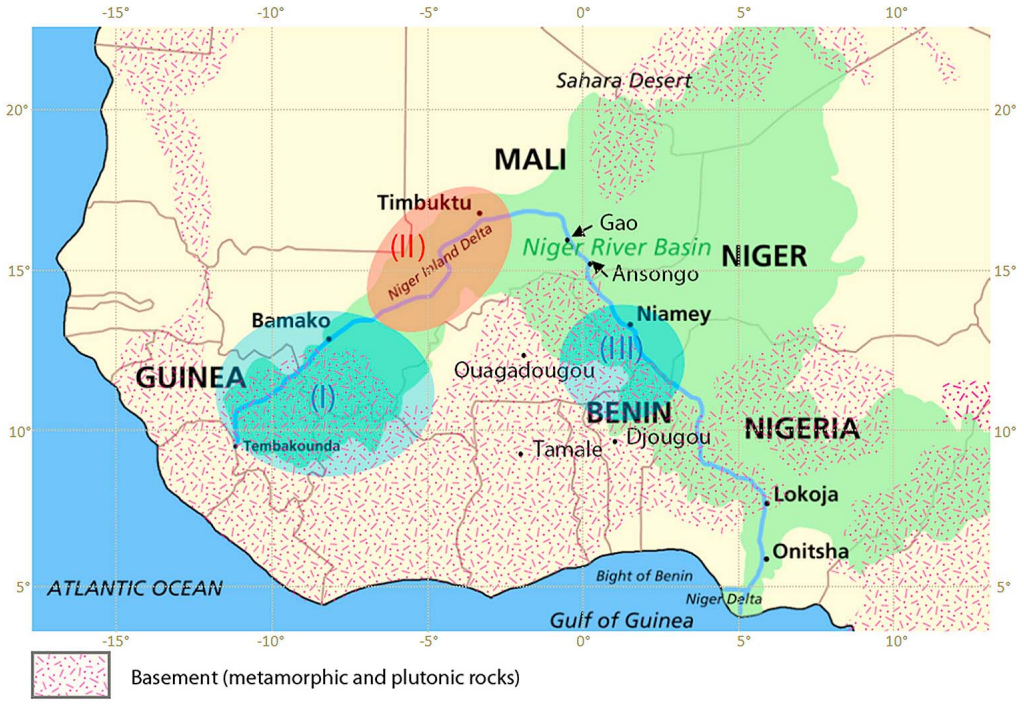

Figure 7. Map of West Africa highlighting the basement rocks (hatched magenta area), the Niger River Basin (green shading), and the Niger River path (blue line). The ellipses indicate: (I) the first drainage basin of the Upper Niger, (II) the Niger Inland Delta, (III) the second drainage basin in the vicinity of Niamey. The basement rocks are commonly overlaid by laterites experience diffuse infiltration toward local aquifers, while sedimentary basins provide large aquifers which recharge through a network of ponds.

later because of a delay due to the filling of the Inland Delta region in area II in Figure 7. The maximum of the water discharge in the Niger River occurs thus in early December at Timbuktu, in late December at Gao and in early January at Niamey (Figure 8). Niamey is located in a more rainy area than the other two sites where a local flood peak, called the "red flood", is seen between June and October, short after the monsoonal rainfalls peak. The red flood is induced by several tributaries of the Niger River in area III in Figure 7 [e.g., *Descroix et al.*, 2009].

[44] Concerning the three other sites, Ouagadougou and Tamale are located in the Volta River basin and Djougou is located in the upper region of the smaller Ouémé River basin. Ouagadougou lies on paleo-proterozoic crystalline and foliated bedrock formations which are covered by a thick weathered zone. In these formations, more or less three aquifer levels can be distinguished but two groundwater tables are generally considered: the superficial water table in laterites and the deep water table, which includes granitic sand and fractured bedrock [*Savadogo*, 1984; *Yameogo*, 2008].

4.2. Coincidence With Surface Water Transport in the Niger River Basin

[45] Figure 8 helps investigating the link between the regional-scale hydrologic loading, the residual GPS signal (considered as representing a local effect) and the discharge of the Niger River at, or close to, the location of the three Sahelian GPS stations. At all three sites, the coincidence between the discharge peak in December and the peak in the residual GPS signal (uplift) is striking.

[46] At Timbuktu and Gao, the residual signal shows a single positive peak but its duration is shorter than that of the mean discharge envelope. The rising part of the mean discharge envelope can be split into two parts, the first one (August–October) having a steeper slope than the second one (October–December). During the first period, rainfall in the Sudano-Sahelian region contributes to infiltration and runoff with two consequences. Infiltration increases soil moisture at regional scale, hence the peak of the hydrologic loading component and the quite good agreement with the subsidence observed by GPS (Figures 8a and 8d). Runoff contributes to the fast increase of water flow in the Niger River. During the second period, soil moisture at regional scale decreases because precipitation drops with the retreat of the monsoon while evapotranspiration is still active [*Meynadier et al.*, 2010a, 2010b]. Nevertheless, the discharge in the Niger River still increases with the arrival of the black flood (Figures 8c and 8f). The uplift observed at the GPS stations during this period actually counter-balances the subsidence induced by the regional-scale loading. A possible mechanism explaining the uplift at the GPS station is the swelling of the soils below the basement of the pillar supporting the antenna. Since the GPS stations are located a few km away from the center of the River channel, some lateral transfer of water is required in the riverbed unless the water flows into a deeper water table extending beneath the station. Swelling is a mechanical reaction of clays to water absorption, and it can

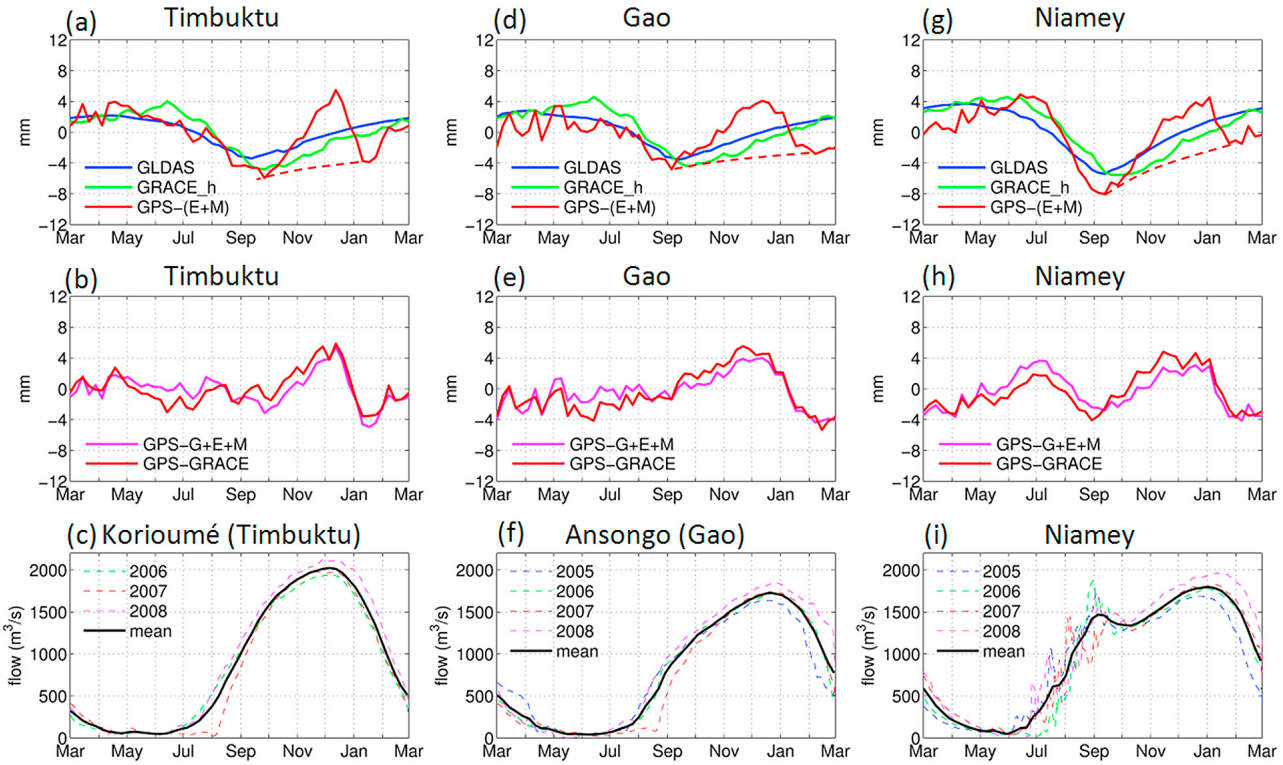

Figure 8. (a) Mean annual hydrological signals at Timbutku from GLDAS (blue curves), GRACE (green curves) and GPS (red curves) where the latter two are derived by subtracting the modeled atmosphere+ ocean components (E+M) from the total deformation estimates, (b) mean annual residual GPS signal (GPS minus sum of models in magenta; GPS minus GRACE in red), (c) discharge (m^3 s^{-1}) of the Niger River at the stream gauge nearest to the GPS station from the NIGER-HYCOS database, (d–f) similar to Figures 8a–8c at Gao, (g–i) similar to Figures 8a–8c at Niamey. The dotted lines in Figures 8a, 8 d, and 8 g represent the GPS loading signal extrapolated in the absence of the uplift/subsidence peak attributed to local pedological effects.

easily induce cm level surface deformations [*Holtz and Kovacs*, 1981]. According to pedological data over the region, the soils of Timbuktu and Gao are composed of sands, clays, laterites, and alluvial sandy loam, which make our hypothesis plausible. The fast subsidence observed between mid-December and mid-January at Timbuktu (or mid-February at Gao) may be due to a shrinkage phase following the swelling phase of the soils. Finally, the negative half-period of the GPS residual oscillation (January–March) might be due to the underestimation of a local loading effect by GRACE and GLDAS compared with GPS. Under this assumption, the hydrological loading signals extrapolated from the GPS data could be represented as the dotted lines in Figures 8a, 8d, and 8g. They differ from the GRACE signals by more than 4 mm. The local loading excess might be due to the water stored in the soil, the aquifer, and the riverbed in the vicinity of the GPS stations. A simple elastic deformation model (invoking Boussinessq equation [see *Holtz and Kovacs*, 1981]) predicts that the loading effect due to the main branch of the Niger River (modeled as a 300 m wide channel) is about 1–2 mm at a distance of less than 5 km during the highest water level period. Since the Niger River is not explicitly represented in GLDAS, these local effects cannot be simulated. But GRACE could be sensitive to the associated mass variations, though the signal may be largely damped because of its coarse spatial resolution. Indeed, GRACE shows a slightly larger hydrological loading than GLDAS between September and March, as well as a delay of 2 weeks. Both these features are consistent with the hypothesis of a small loading effect linked with flooding in the Niger riverbed.

[47] At Niamey, the same hypotheses can be made about the coincidence of the black flood and the September-to-March oscillation in the residual GPS signal. Similarly, the first oscillation peaking in July might be explained by swelling of soils due to the red flood. The fact that the phases do not match perfectly between these signals might be due to the superposition of various effects (both local and regional loadings, and local swelling/shrinking).

4.3. Coincidence With Water Table Variations in Ouagadougou

[48] Since the estimated GPS vertical deformation in Ouagadougou shows an additional signal similar to the one observed at the three sites located along the Niger River, we sought for a similar explanation involving a local source of water. Ouagadougou is actually surrounded by four dams, which are drained by channels from the tributaries of the Massili, the main river crossing the city [*Yameogo*, 2008]. Fortunately, data from hydrological and geological surveys

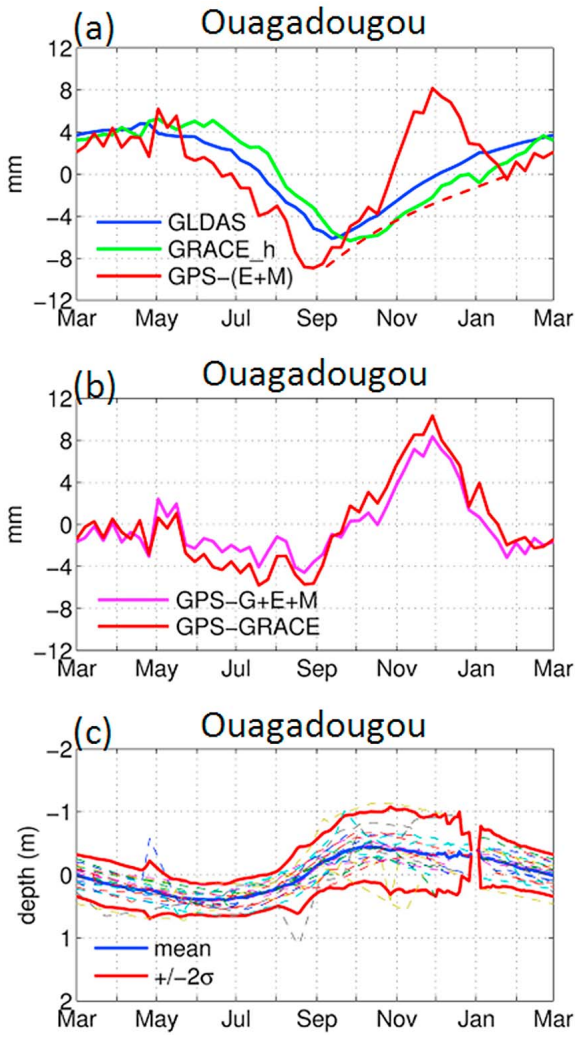

Figure 9. (a, b) Similar to Figures 8a and 8b but for Ouagadougou, (c) mean seasonal variation of the water table depth of the lateritic aquifer in Ouagadougou measured by a nearby piezometer from CIEH over the 1978–2004 period (each year is represented by a thin dashed line; overall mean by thick blue line, and the ±2 standard deviations by the thick red curves).

are available and enable us to perform a more quantitative analysis than for the previous three stations.

[49] The GPS station in Ouagadougou is located at less than 2 km from a 20 m depth piezometer of the Comité Interafrican d'Etudes Hydrauliques (CIEH), which measures the water table height of the lateritic aquifer. At the GPS station, the altitude of the bedrock is about 274 m with a weathered zone 31 m thick [*Yameogo*, 2008]. It is fairly consistent with a survey at the CIEH piezometer site giving the altitude of the bedrock at 270 m with a weathered zone of 28 m. We first used the historical CIEH data available over the 1978–2004 period to determine the seasonal variations of the water table height (Figure 9c). The estimated amplitude of the mean seasonal variation is ∼1 m whereas it can reach ∼2 m during extreme years (e.g. 1991, 1999 and 2003 where the annual precipitation exceeded 800 mm). During the period of our study (2006–2008), the piezometric data were not continuous and cannot be used to characterize the annual cycle. Instead, we extrapolated the water table height variations from the historical data using a scaling based on annual precipitation. It gave an estimate of 1.8 m for the 2006–2008 period.

[50] *Bazie et al.* [1995] provided a lithologic cross section for a measurement point located at the East of Ouagadougou which gives a percentage of clay particles in laterite layers in the range of 23% to 44%. Kaolinite is the dominant clay particle in the soils there. Its activity is between 0.3 and 0.5 [*Skempton*, 1953]. Considering an average percentage of 35% of clay particles, the potential swelling is ∼1% according to *Seed et al.* [1962]. We thus estimate the amplitude of the swelling effect to be about 1.8 m × 0.01 = 0.018 m. This is a straightforward estimate but it is fairly consistent with the amplitude of the observed residual GPS vertical displacement at Ouagadougou of 12 to 16 mm, depending on which of GRACE or the models is subtracted (Figure 9b). A more accurate estimation of the effect would imply to take into account the impact of the other particles composing the soil and the permeability effects of clays in the presence of changes in water content. The complexity of the underlying mechanisms as well as the competition between loading and swelling/shrinking effects might be the reason for the phase lag seen between the water table depth and the GPS residual signal.

5. Summary and Conclusions

[51] This is the first study using three-dimensional ground deformations estimated from GPS data to investigate hydrological loading effects associated with the West African Monsoon. The strong seasonality in precipitation induced by the monsoon system is shown to produce a regional-scale loading effect (subsidence) between 10 and 15 mm across the North-South climatic gradient where the AMMA GPS stations were installed. The vertical component of the GPS displacements shows a daily repeatability comprised between 2 mm during the dry season and 5–6 mm during the wet season, with a median value smaller than 4 mm. This level of accuracy gives good confidence into the ground deformation estimated from GPS data. The vertical deformation component estimated by GPS is actually fairly consistent with regional-scale estimates from GRACE satellite products and geophysical models. The horizontal deformation components are also shown to reflect the loading induced by the monsoon in the sense that they point toward the center of mass of the groundwater anomaly (Sudano-Guinean region). However, this signal is much smaller than the vertical and reaches only 3–4 mm at Niamey for the N component and 1 mm for the E component as estimated by GRACE. The N component of the GPS displacement is consistent with GRACE and the models but the E component of the GPS displacement seems dominated by noise.

[52] A spectral analysis highlights several peaks at annual and subannual frequencies in the vertical deformation. The models show that hydrology is the dominant contributor to the annual harmonic of the loading signal in the Sudanian and Sahelian regions whereas atmospheric loading is dominant over the Sahara. As expected from surface pressure and soil

moisture, the atmospheric loading component increases from south to north whereas the hydrologic component increases toward the south.

[53] The most striking result was that the semiannual harmonics of the GPS deformation is 2–3 times larger than the corresponding GRACE and model estimates. This is due to an additional signal in the GPS deformation series which takes the form of an oscillation occurring between September and March. This oscillation is observed at most of the West African sites, but especially at the Sahelian sites where it reaches 12 to16 mm at Ouagadougou. Though state-of-the-art GPS data processing was used, it cannot be totally excluded that this signal is an artifact from the GPS technique. However, an analysis of the hydro-geological properties of the sites revealed a strong coincidence between the residual GPS signal and flooding at three sites located along the Niger River (Timbuktu, Gao, and Niamey). At Ouagadougou, similar coincidence is found with the seasonal variations of the water table depth. The mechanism proposed to explain the GPS residual signal is a sequence of swelling/shrinking of clays which dominates the associated local loading effects. These local loading effects are partly captured by GRACE but they are strongly damped because of the coarse resolution of the satellite. The swelling/shrinking affects the soil volume and cannot be detected from GRACE measurements. The geophysical models used here are not suited to represent either of these nonloading processes. This case study suggests that beyond their capability to validate GRACE and model estimates at seasonal and sub-seasonal timescales, nonlinear GPS ground deformation estimates may help diagnosing subtle local hydro-geological processes.

[54] It seems difficult to further test the hypothesized mechanism to explain the observed GPS residual signal from data available in West Africa. It may be tested at a few stations in the global GPS network which show similar GPS residuals with respect to GRACE deformation estimates. More generally, the hydro-geological processes such as those suggested in this study might explain part of the so-far unexplained strong periodic signals observed in many GPS position estimates.

[55] **Acknowledgments.** The authors would like to thank Jacques Chedhomme (ENSG, Institut Géographique National, Marne La Vallée, France) for meaningful discussion on geological processes in Africa and Tonie M. van Dam (Faculté des Sciences, de la Technologie et de la Communication, University of Luxembourg, Luxembourg) for providing geophysical model products that were used as an independent data set for the validation of the model products used in this manuscript. The SONEL (www.sonel.org) data assembly center is also acknowledged for providing useful, comprehensive, access to GPS data from many supporting agencies and individuals worldwide.

References

Altamimi, Z., and X. Collilieux (2009), IGS contribution to ITRF, *J. Geod.*, *83*(3–4), 375–383, doi:10.1007/s00190-008-0294-x.

Altamimi, Z., X. Collilieux, J. Legrand, B. Garayt, and C. Boucher (2007), ITRF2005: A new release of the International Terrestrial Reference Frame based on time series of station positions and Earth orientation parameters, *J. Geophys. Res.*, *112*, B09401, doi:10.1029/2007JB004949.

Bazie, P., B. Dieng, and P. Ackerer (1995), Bilan des transferts verticaux d'eau en zone non-saturée sous climat soudano-sahélien: Application à l'estimation de la recharge des nappes (in French), *Rev. Sci. Eau*, *8*(2), 237–260.

Blewitt, G. (2003), Self-consistency in reference frames, geocenter definition, and surface loading of the solid Earth, *J. Geophys. Res.*, *108*(B6), 2103, doi:10.1029/2002JB002082.

Bock, O., et al. (2008), The West African Monsoon observed by ground-based GPS receivers during the AMMA project, *J. Geophys. Res.*, *113*, D21105, doi:10.1029/2008JD010327.

Boehm, J., B. Werl, and H. Schuh (2006), Troposphere mapping functions for GPS and very long baseline interferometry from European Centre for Medium-Range Weather Forecasts operational analysis data, *J. Geophys. Res.*, *111*, B02406, doi:10.1029/2005JB003629.

Boone, A., et al. (2009), The AMMA Land Surface Model Intercomparison Project (ALMIP), *Bull. Am. Meteorol. Soc.*, *90*(12), 1865–1880, doi:10.1175/2009BAMS2786.1.

Bruinsma, S., J. M. Lemoine, R. Biancale, and N. Vales (2010), CNES/GRGS 10-day gravity field models (release 2) and their evaluation, *Adv. Space Res.*, *45*, 587–601, doi:10.1016/j.asr.2009.10.012.

Carrère, L., and F. Lyard (2003), Modeling the barotropic response of the global ocean to atmospheric wind and pressure forcing: Comparisons with observations, *Geophys. Res. Lett.*, *30*(6), 1275, doi:10.1029/2002GL016473.

Chen, F., K. Mitchell, J. Schaake, Y. Xue, H.-L. Pan, V. Koren, Q. Duan, M. Ek, and A. Betts (1996), Modeling of land surface evaporation by four schemes and comparison with FIFE observations, *J. Geophys. Res.*, *101*(D3), 7251–7268, doi:10.1029/95JD02165.

Collilieux, X., L. Metivier, Z. Altamimi, T. van Dam, and J. Ray (2011a), Quality assessment of GPS reprocessed terrestrial reference frame, *GPS Solut.*, *15*(3), 219–231, doi:10.1007/s10291-010-0184-6.

Collilieux, X., T. van Dam, J. Ray, D. Coulot, L. Metivier, and Z. Altamimi (2011b), Strategies to mitigate aliasing of loading signals while estimating GPS frame parameters, *J. Geod.*, *86*, 1–14, doi:10.1007/s00190-011-0487-6.

Crowley, J., J. Mitrovica, R. Bailey, M. Tamisiea, and J. Davis (2006), Land water storage within the Congo Basin inferred from GRACE satellite gravity data, *Geophys. Res. Lett.*, *33*, L19402, doi:10.1029/2006GL027070.

Crowley, J., J. Mitrovica, R. Bailey, M. Tamisiea, and J. Davis (2008), Annual variations in water storage and precipitation in the Amazon basin, *J. Geod.*, *82*, 9–13, doi:10.1007/s00190-007-0153-1.

Dach, R., J. Boehm, S. Lutz, P. Steigenberger, and G. Beutler (2011), Evaluation of the impact of atmospheric pressure loading model on GNSS data analysis, *J. Geod.*, *85*, 75–91, doi:10.1007/s00190-010-0417-z.

Davis, J. L., P. Elosegui, J. X. Mitrovica, and M. E. Tamisiea (2004), Climate-driven deformation of the solid Earth from GRACE and GPS, *Geophys. Res. Lett.*, *31*, L24605, doi:10.1029/2004GL021435.

Dee, D., et al. (2011), The ERA-Interim reanalysis: Configuration and performance of the data assimilation system, *Q. J. R. Meteorol. Soc.*, *137*, 553–597, doi:10.1002/qj.828.

Desconnets, J. C., J. D. Taupin, T. Lebel, and C. Leduc (1997), Hydrology of the HAPEX-Sahel Central Supersite: Surface water drainage and aquifer recharge through the pool systems, *J. Hydrol.*, *188-189*(1–4), 155–178, doi:10.1016/S0022-1694(96)03158-7.

Descroix, L., et al. (2009), Spatio-temporal variability of hydrological regimes around the boundaries between Sahelian and Sudanian areas of West Africa: A synthesis, *J. Hydrol.*, *375*(1–2), 90–102, doi:10.1016/j.jhydrol.2008.12.012.

Dong, D., P. Fang, Y. Bock, M. K. Cheng, and S. Miyazaki (2002), Anatomy of apparent seasonal variations from GPS-derived site position time series, *J. Geophys. Res.*, *107*(B4), 2075, doi:10.1029/2001JB000573.

Dong, D., T. Yunck, and M. Heflin (2003), Origin of the ITRF, *J. Geophys. Res.*, *108*(B4), 2200, doi:10.1029/2002JB002035.

Dow, J. M., R. E. Neilan, and C. Rizos (2009), The International GNSS Service in a changing landscape of Global Navigation Satellite Systems, *J. Geod.*, *83*, 191–198, doi:10.1007/s00190-008-0300-3.

Dziewonski, A. M., and D. L. Anderson (1981), Preliminary reference Earth model, *Phys. Earth Planet. Inter.*, *25*, 297–356, doi:10.1016/0031-9201(81)90046-7.

Ek, M., K. Mitchell, Y. Lin, P. Grummann, V. Koren, G. Gayno, and J. Tarpley (2003), Implementation of Noah land surface model advances in the National Centers for Environmental Prediction operational mesoscale Eta model, *J. Geophys. Res.*, *108*(D22), 8851, doi:10.1029/2002JD003296.

Farrell, W. E. (1972), Deformation of the Earth by surface loads, *Rev. Geophys.*, *10*(3), 761–797, doi:10.1029/RG010i003p00761.

Favreau, G., B. Cappelaere, S. Massuel, M. Leblanc, M. Boucher, N. Boulain, and C. Leduc (2009), Land clearing, climate variability, and water resources increase in semiarid southwest Niger: A review, *Water Resour. Res.*, *45*, W00A16, doi:10.1029/2007WR006785.

Ferland, R. (2010), Combination of the reprocessed IGS Analysis Center SINEX solutions, paper presented at the IGS Workshop 2010, Newcastle upon Tyne, UK, 28 June to 2 July.

Greigert, J. (1968), Les eaux souterraines de la République du Niger, *Rep. 68(AB1 006 NIA)*, 407 pp., Bur. de Rech. Géol. et Min., Orléans, France.

Grippa, M., et al. (2011), Land water storage variability over West Africa estimated by Gravity Recovery and Climate Experiment (GRACE) and land surface models, *Water Resour. Res.*, *47*, W05549, doi:10.1029/2009WR008856.

Güntner, A. (2008), Improvement of global hydrological models using GRACE data, *Surv. Geophys.*, *29*, 375–397, doi:10.1007/s10712-008-9038-y.

Han, S.-C., I.-Y. Yeo, D. Alsdorf, P. Bates, J.-P. Boy, H. Kim, T. Oki, and M. Rodell (2010), Movement of Amazon surface water from time-variable satellite gravity measurements and implications for water cycle parameters in land surface models, *Geochem. Geophys. Geosyst.*, *11*, Q09007, doi:10.1029/2010GC003214.

Hernandez-Pajares, M., J. Juan, J. Sanz, and R. Orus (2007), Second-order ionospheric term in GPS: Implementation and impact on geodetic estimates, *J. Geophys. Res.*, *112*, B08417, doi:10.1029/2006JB004707.

Herring, T. A., R. W. King, and S. C. McClusky (2008), Introduction to GAMIT/GLOBK, report, Mass. Inst. of Technol., Cambridge. [Available at http://www-gpsg.mit.edu/~simon/gtgk/docs.htm.]

Hinderer, J., et al. (2009), The GHYRAF (Gravity and Hydrology in Africa) experiment: Description and first results, *J. Geodyn.*, *48*, 172–181, doi:10.1016/j.jog.2009.09.014.

Hinderer, J., et al. (2011), Land water storage changes from ground and space geodesy: First results from the GHYRAF (Gravity and Hydrology in Africa) experiment, *Pure Appl. Geophys.*, doi:10.1007/s00024-011-0417-9, in press.

Holtz, R. D., and W. D. Kovacs (1981), *An Introduction to Geotechnical Engineering*, 733 pp., Prentice Hall, Englewood Cliffs, N. J.

Huffman, G., et al. (1997), The Global Precipitation Climatology Project (GPCP) combined precipitation dataset, *Bull. Am. Meteorol. Soc.*, *78*, 5–20, doi:10.1175/1520-0477(1997)078<0005:TGPCPG>2.0.CO;2.

Jacks, G., and M. Traoré (2008), Mechanisms and rates of recharge at Timbuktu (Republic of Mali), in *Groundwater for Sustainable Development: Problems, Perspectives and Challenges*, edited by P. Bhattachary et al., pp. 55–60, Taylor and Francis, London.

King, M. A., and C. S. Watson (2010), Long GPS coordinate time series: Multipath and geometry effects, *J. Geophys. Res.*, *115*, B04403, doi:10.1029/2009JB006543.

King, M., P. Moore, P. Clarke, and D. Lavallée (2006), Choice of optimal averaging radii for temporal GRACE gravity solutions, a comparison with GPS and satellite altimetry, *Geophys. J. Int.*, *166*, 1–11, doi:10.1111/j.1365-246X.2006.03017.x.

King, M. A., C. S. Watson, N. T. Penna, and P. J. Clarke (2008), Subdaily signals in GPS observations and their effect at semiannual and annual periods, *Geophys. Res. Lett.*, *35*, L03302, doi:10.1029/2007GL032252.

Kouba, J. (2008), Implementation and testing of the gridded Vienna mapping function 1 (VMF1), *J. Geod.*, *82*(4–5), 193–205, doi:10.1007/s00190-007-0170-0.

Kusche, J., and E. J. O. Schrama (2005), Surface mass redistribution inversion from global GPS deformation and GRACE gravity data, *J. Geophys. Res.*, *110*, B09409, doi:10.1029/2004JB003556.

L'Hote, Y., and G. Mahé (1996), Afrique centrale et de l'ouest: Carte des précipitations moyennes annuelles (période 1951–1989), Inst. de Rech. pour le Dév., Bondy, France. [Available at http://www.cartographie.ird.fr/pluvio.html.]

Lavaysse, C., C. Flamant, S. Janicot, D. J. Parker, J.-P. Lafore, B. Sultan, and J. Pelon (2009), Seasonal evolution of the West African heat low: A climatological perspective, *Clim. Dyn.*, *33*, 313–330, doi:10.1007/s00382-009-0553-4.

Lebel, T., et al. (2009), The AMMA-CATCH studies in the Sahelian region of West-Africa: An overview, *J. Hydrol.*, *375*, 3–13, doi:10.1016/j.jhydrol.2009.03.020.

Lyard, F., F. Lefevre, T. Letellier, and O. Francis (2006), Modelling the global ocean tides: Modern insights from FES2004, *Ocean Dyn.*, *56*, 394–415, doi:10.1007/s10236-006-0086-x.

Métivier, L., M. Greff-Lefftz, and M. Diament (2005), A new approach to computing accurate gravity time variations for a realistic earth model with lateral heterogeneities, *Geophys. J. Int.*, *162*, 570–574, doi:10.1111/j.1365-246X.2005.02692.x.

Meynadier, R., O. Bock, F. Guichard, A. Boone, P. Roucou, and J.-L. Redelsperger (2010a), West African Monsoon water cycle: 1. A hybrid water budget data set, *J. Geophys. Res.*, *115*, D19106, doi:10.1029/2010JD013917.

Meynadier, R., O. Bock, S. Gervois, F. Guichard, J.-L. Redelsperger, A. Agustí-Panareda, and A. Beljaars (2010b), West African Monsoon water cycle: 2. Assessment of numerical weather prediction water budgets, *J. Geophys. Res.*, *115*, D19107, doi:10.1029/2010JD013919.

Munekane, H. (2007), Ocean mass variations from GRACE and tsunami gauges, *J. Geophys. Res.*, *112*, B07403, doi:10.1029/2006JB004618.

Panet, I., F. Pollitz, V. Mikhailov, M. Diament, P. Banerjee, and K. Grijalva (2010), Upper mantle rheology from GRACE and GPS postseismic deformation after the 2004 Sumatra-Andaman earthquake, *Geochem. Geophys. Geosyst.*, *11*, Q06008, doi:10.1029/2009GC002905.

Penna, N. T., and M. P. Stewart (2003), Aliased tidal signatures in continuous GPS height time series, *Geophys. Res. Lett.*, *30*(23), 2184, doi:10.1029/2003GL018828.

Penna, N. T., M. A. King, and M. P. Stewart (2007), GPS height time series: Short-period origins of spurious long-period signals, *J. Geophys. Res.*, *112*, B02402, doi:10.1029/2005JB004047.

Petrie, E. J., M. A. King, P. Moore, and D. A. Lavallée (2010), Higher-order ionospheric effects on the GPS reference frame and velocities, *J. Geophys. Res.*, *115*, B03417, doi:10.1029/2009JB006677.

Petrov, L., and J.-P. Boy (2004), Study of the atmospheric pressure loading signal in very long baseline interferometry observations, *J. Geophys. Res.*, *109*, B03405, doi:10.1029/2003JB002500.

Press, W. H., S. A. Teukolsky, W. T. Vetterling, and B. P. Flannery (1992), *Numerical Recipes in FORTRAN 77: The Art of Scientific Computing*, 2nd ed., 933 pp., Cambridge Univ. Press, New York.

Ramillien, G., F. Frappart, A. Cazenave, and A. Guntner (2005), Time variations of land water storage from an inversion of 2 years of GRACE geoids, *Earth Planet. Sci. Lett.*, *235*, 283–301, doi:10.1016/j.epsl.2005.04.005.

Ray, J., Z. Altamimi, X. Collilieux, and T. Van Dam (2008), Anomalous harmonics in the spectra of GPS position estimates, *GPS Solut.*, *12*(1), 55–64, doi:10.1007/s10291-007-0067-7.

Reager, J., and J. Famiglietti (2009), Global terrestrial water storage capacity and flood potential using GRACE, *Geophys. Res. Lett.*, *36*, L23402, doi:10.1029/2009GL040826.

Redelsperger, J.-L., C. Thorncroft, A. Diedhiou, T. Lebel, D. J. Parker, and J. Polcher (2006), African Monsoon Multidisciplinary Analysis (AMMA): An international research project and field campaign, *Bull. Am. Meteorol. Soc.*, *87*, 1739–1746, doi:10.1175/BAMS-87-12-1739.

Rodell, M., et al. (2004), The global land data assimilation system, *Bull. Am. Meteorol. Soc.*, *85*(3), 381–394, doi:10.1175/BAMS-85-3-381.

Saad, K. (1971), Etude hydrogéologique du nord de la boucle du Niger, *Rep. 2257/RMS.RS/SCE*, 49 pp., U. N. Educ. Sci. and Cult. Org., Paris.

Santamaría-Gómez, A., M. N. Bouin, X. Collilieux, and G. Wöppelmann (2011), Correlated errors in GPS position time series: Implications for velocity estimates, *J. Geophys. Res.*, *116*, B01405, doi:10.1029/2010JB007701.

Santamaría Gómez, A., M.-N. Bouin, and G. Wöppelmann (2012), Improved GPS data analysis strategy for tide gauge benchmark monitoring, in *Geodesy for Planet Earth: IAG Symposia*, vol. 136, edited by S. Kenyon et al., pp. 11–18, Springer, Berlin, doi:10.1007/978-3-642-20338-1_2.

Savadogo, A. N. (1984), Géologie et hydrogéologie du socle cristallin de Haute-Volta: Etude régionale du bassin versant de la Sissili, PhD thesis, Univ. of Grenoble I, Grenoble, France.

Schmid, R., P. Steigenberger, G. Gendt, M. Ge, and M. Rothacher (2007), Generation of a consistent absolute phase-center correction model for GPS receiver and satellite antennas, *J. Geod.*, *81*, 781–798, doi:10.1007/s00190-007-0148-y.

Schmidt, R., et al. (2006), GRACE observations of changes in continental water storage, *Global Planet. Change*, *50*, 112–126, doi:10.1016/j.gloplacha.2004.11.018.

Schmidt, R., S. Petrovic, A. Guntner, F. Barthelmes, J. Wunsch, and J. Kusche (2008), Periodic components of water storage changes from GRACE and global hydrology models, *J. Geophys. Res.*, *113*, B08419, doi:10.1029/2007JB005363.

Seed, H. B., R. J. Woodward, and R. Lundgren (1962), Prediction of swelling potential for compacted clays, *J. Soil Mech. Found. Div. Am. Soc. Civ. Eng.*, *88*(SM3), 53–87.

Seguis, L., et al. (2011), Origins of streamflow in a crystalling basement catchment in a sub-humid Sudanian zone: the Donga basin (Benin, West Africa): Inter-annual variability of water budget, *J. Hydrol.*, *402*, 1–13, doi:10.1016/j.jhydrol.2011.01.054.

Skempton, A. W. (1953), The colloidal activity of clays, in *Proceedings of the Third International Conference on Soil Mechanics and Foundation Engineering*, vol. I, p. 57–61, Int. Soc. Soil Mech. and Found. Eng., London.

Steckler, M. S., S. L. Nooner, S. H. Akhter, S. K. Chowdhury, S. Bettadpur, L. Seeber, and M. G. Kogan (2010), Modeling Earth deformation from monsoonal flooding in Bangladesh using hydrographic, GPS, and Gravity Recovery and Climate Experiment (GRACE) data, *J. Geophys. Res.*, *115*, B08407, doi:10.1029/2009JB007018.

Syed, T. H., J. S. Famiglietti, M. Rodell, J. Chen, and C. R. Wilson (2008), Analysis of terrestrial water storage changes from GRACE and GLDAS, *Water Resour. Res.*, *44*, W02433, doi:10.1029/2006WR005779.

Tapley, B., S. Bettadpur, J. Ries, P. Thompson, and M. Watkins (2004), GRACE measurements of mass variability in the Earth system, *Science*, *305*, 503–505, doi:10.1126/science.1099192.

Tardy, Y. (1997), *Petrology of Laterites and Tropical Soils*, 409 pp., A. A. Balkema, Rotterdam, Netherlands.

Tesmer, V., P. Steigenberger, T. van Dam, and T. Mayer-Gurr (2011), Vertical deformations from homogeneously processed GRACE and global GPS long-term series, *J. Geod.*, *85*, 291–310, doi:10.1007/s00190-010-0437-8.

Tregoning, P., and T. van Dam (2005), Effects of atmospheric pressure loading and seven parameter transformations on estimates of geocenter motion and station heights from space geodetic observations, *J. Geophys. Res.*, *110*, B03408, doi:10.1029/2004JB003334.

Tregoning, P., and C. Watson (2009), Atmospheric effects and spurious signals in GPS analyses, *J. Geophys. Res.*, *114*, B09403, doi:10.1029/2009JB006344.

Tregoning, P., and C. Watson (2011), Correction to "Atmospheric effects and spurious signals in GPS analyses," *J. Geophys. Res.*, *116*, B02412, doi:10.1029/2010JB008157.

Tregoning, P., C. Watson, G. Ramillien, H. McQueen, and J. Zhang (2009), Detecting hydrologic deformation using GRACE and GPS, *Geophys. Res. Lett.*, *36*, L15401, doi:10.1029/2009GL038718.

Uppala, S. M., et al. (2005), The ERA-40 re-analysis, *Q. J. R. Meteorol. Soc.*, *131*, 2961–3012, doi:10.1256/qj.04.176.

van Dam, T., J. Wahr, and D. Lavallee (2007), A comparison of annual vertical crustal displacements from GPS and GRACE over Europe, *J. Geophys. Res.*, *112*, B03404, doi:10.1029/2006JB004335.

Wahr, J., M. Molenaar, and F. Bryan (1998), Time variability of the Earth's gravity field: Hydrological and oceanic effects and their possible detection using GRACE, *J. Geophys. Res.*, *103*, 30,205–30,229, doi:10.1029/98JB02844.

Wahr, J., S. Swenson, V. Zlotnicki, and I. Velicogna (2004), Time-variable gravity from GRACE: First results, *Geophys. Res. Lett.*, *31*, L11501, doi:10.1029/2004GL019779.

Williams, S. D. P., and N. T. Penna (2011), Non-tidal ocean loading effects on geodetic GPS heights, *Geophys. Res. Lett.*, *38*, L09314, doi:10.1029/2011GL046940.

Wu, X., X. Collilieux, and Z. Altamimi (2010), Data sets and inverse strategies for global surface mass variations, *Geophys. Res. Abstr.*, *12*, EGU5484.

Xie, P., J. Janowlak, P. Arkin, R. Adler, A. Gruber, R. Ferraro, G. Huffman, and S. Curtis (2003), GPCP Pentad precipitation analyses: An experimental dataset based on gauge observations and satellite estimates, *J. Clim.*, *16*, 2197–2214, doi:10.1175/2769.1.

Yameogo, S. (2008), Ressources en eau souterraine du centre urbain de Ouagadougou au Burkina Faso, qualité et vulnérabilité, PhD thesis, Univ. of Avignon and the Vaucluse, Avignon, France.

Yan, H., W. Chen, Y. Zhu, W. Zhang, and M. Zhong (2009), Contributions of thermal expansion of monuments and nearby bedrock to observed GPS height changes, *Geophys. Res. Lett.*, *36*, L13301, doi:10.1029/2009GL038152.